Gi-Chul Yang · Sio-Iong Ao
Len Gelman *Editors*

Transactions on Engineering Technologies

Special Volume of the World Congress on Engineering 2013

Springer

Transactions on Engineering Technologies

Gi-Chul Yang · Sio-Iong Ao
Len Gelman
Editors

Transactions on Engineering Technologies

Special Volume of the World Congress on Engineering 2013

Springer

Editors
Gi-Chul Yang
Department of Multimedia Engineering,
College of Engineering
Mokpo National University
Mokpo, Jeonnam
Republic of Korea

Len Gelman
Department of Applied Mathematics
and Computing
Cranfield University
Cranfield, Bedfordshire
UK

Sio-Iong Ao
IAENG Secretariat
International Association of Engineers
Hong Kong
Hong Kong SAR

ISBN 978-94-017-8831-1 ISBN 978-94-017-8832-8 (eBook)
DOI 10.1007/978-94-017-8832-8
Springer Dordrecht Heidelberg New York London

Library of Congress Control Number: 2013953195

Printed on acid-free paper

Springer is part of Springer Science+Business Media (www.springer.com)

Preface

A large international conference on Advances in Engineering Technologies and Physical Science was held in London, U.K., 3–5 July, 2013, under the World Congress on Engineering 2013 (WCE 2013). The WCE 2013 is organized by the International Association of Engineers (IAENG); the Congress details are available at: http://www.iaeng.org/WCE2013. IAENG is a nonprofit international association for engineers and computer scientists, which was founded originally in 1968. The World Congress on Engineering serves as good platforms for the engineering community to meet with each other and to exchange ideas. The conferences have also struck a balance between theoretical and application development. The conference committees have been formed with over 300 committee members who are mainly research center heads, faculty deans, department heads, professors, and research scientists from over 30 countries. The Congress is truly an international meeting with a high level of participation from many countries. The response to the Congress has been excellent. There have been more than 1,100 manuscript submissions for the WCE 2013. All submitted papers have gone through the peer review process, and the overall acceptance rate is 55.12 %.

This volume contains 48 revised and extended research articles written by prominent researchers participating in the conference. Topics covered include mechanical engineering, bioengineering, Internet engineering, image engineering, wireless networks, knowledge engineering, manufacturing engineering, and industrial applications. The book offers the state of art of tremendous advances in engineering technologies and physical science and applications, and also serves as an excellent reference work for researchers and graduate students working on engineering technologies and physical science and applications.

Gi-Chul Yang
Sio-Iong Ao
Len Gelman

Contents

Viscous Fingering of Reversible Reactive Flows in Porous Media

Hesham Alhumade and Jalel Azaiez

Abstract The dynamics of viscous fingering instability of miscible displacements in a homogeneous porous medium are examined in the case of flows that involve reversible chemical reactions between the displacing and displaced fluid. The flows are modeled using the continuity equation, Darcy's law, and volume-averaged forms of the convection-diffusion-reaction equation for mass balance of a bi-molecular reaction. Numerical simulations were carried out using a Hartley transform based pseudo-spectral method combined with semi-implicit finite-difference time-stepping algorithm. The results of the simulations allowed to analyze the mechanisms of fingering instability that result from the dependence of the fluids viscosities on the concentrations of the different species, and focused on different flow scenarios. In particular, the study examined the effects of varying important parameters namely the Damkohler number that represents the ratio of the hydrodynamic and chemical characteristic time scales, and the chemical reversibility coefficient, and analyzed the resulting changes in the finger structures. The results are presented for flows with an initially stable as well as initially unstable front between the two reactants.

Keywords Fluid mechanics · Homogeneous porous media · Hydrodynamics · Miscible displacements · Reversible chemical reaction · Stability · Viscous fingering

H. Alhumade
University of Waterloo, 200 University Avenue West Waterloo, Waterloo, ON N2L 3G1, Canada
e-mail: halhumade@uwaterloo.ca

J. Azaiez (✉)
University of Calgary, 2500 University Dr. NW Calgary, Calgary, Alberta T2N 1N4, Canada
e-mail: azaiez@ucalgary.ca

G.-C. Yang et al. (eds.), *Transactions on Engineering Technologies*,
DOI: 10.1007/978-94-017-8832-8_1,

1 Introduction

When a viscous fluid is used to displace another one of a larger viscosity, a frontal instability appears at the interface between the two fluids, which may dramatically affect the overall efficiency of the displacement process. This instability may grow to form fingers that propagate in both upstream and downstream directions and is referred to as fingering or Saffman–Taylor instability [21]. The instability can be triggered by either viscosity mismatch and is referred to as viscous fingering or density mismatch, where it is known as the Rayleigh-Taylor instability. Such instabilities are encountered in a wide variety of processes that include enhanced oil recovery, soil remediation, chromatography and CO_2 sequestration. Many experimental and theoretical studies have focused on the frontal instability of non-reactive displacement processes, where hydrodynamic interactions between the fluids result in the viscous fingering instability. In these studies the effects of different parameters were examined and most of these studies were reviewed in [11, 13].

The viscous fingering instability may develop in conjunction with chemical reactions in a wide variety of processes such as underground water treatment, tertiary heavy oil recovery, spreading of chemical pollutants chromatographic separation, polymer synthesis and processing as well as fixed bed regeneration [14]. There has been a growing interest in analyzing such reactive flow instability and a number of studies have examined the reactive flow. One of the earliest studies of reactive displacements in porous media was conducted out by [19], where the reaction leads to an interfacial tension decrease in a secondary oil recovery process. A number of subsequent experimental studies examined the effects of different parameters such as stoichiometry [16], geometry orientation [12], finger growth rate [17], chemical composition [3], external electrical field [25], variation in the physical properties of the phases [20], and precipitation [18].

Analytical and numerical Modelling of reactive flow displacements has been carried out by a limited, but growing number of studies [6–10]. These studies have considered either auto-catalytic or non-autocatalytic reactions.

All existing studies dealing with reactive viscous fingering have assumed the chemical reaction to be complete. However the reversibility of the reaction plays an important role in many phenomena studied in physics, chemistry, biology, and geology [9]. For example, in the in situ soil remediation, promising results were reported by [26], where a reactive fluid was injected to remove the pollutant from the underground water. The first study on reactive-diffusive systems with reversible reaction was carried out by [5], where the properties of a reversible reactive front with initially separated reactants were examined. It was reported that the dynamics of the reactive front can be described as a crossover between irreversible and reversible regimes at short and long times, respectively. A subsequent study [23] confirmed the existence of a crossover between short time “irreversible” and long-time “reversible” regimes. In a recent study [22], the reaction rate of a reversible reactive-diffusive process when the reactants are initially mixed with

different diffusion coefficients by using the boundary layer function method was investigated. The authors reported that the reactive-diffusive process for this case can be considered as a quasi-equilibrium process and analyzed the dependence of the reaction rate on the initial distribution of the reactants.

It should be noted that even though the above studies did examine the role of chemical reversibility, there conclusions are actually very restrictive since they accounted only for diffusive effects. It is however known that in actual flow displacements that involve the injection of chemical species; convective effects must be included in the model to analyze properly the flow. Actually, for such flows convective effects can be dominant at least at some stages of the flow and hence cannot be ignored. Motivated by this, the first linear stability analysis to understand the effects of chemical reversibility on the stability of some cases of reactive-diffusive-convective flow displacements [1]. In a recent study, the role of chemical reversibility on the stability of some cases of reactive-diffusive-convective flow displacements was investigated [2]. In this study, the nonlinear development of the flow are analyzed through numerical simulations.

2 Mathematical Model

2.1 Physical Problem

A two-dimensional displacement is considered in which both fluids are incompressible and fully miscible. The flow takes place in horizontal direction in a homogeneous medium of constant porosity ϕ and permeability K. A schematic of the two-dimensional porous medium is shown in Fig. 1. The length, width and thickness (z-direction) of the medium are L_x, L_y and b respectively.

The medium is assumed to be initially filled with a solution of a reactant (B) of viscosity μ_B. A miscible fluid (A) of viscosity μ_A is injected from the left-hand side with a uniform velocity U to displace fluid (B). The direction of the flow is along the x-axis and the y-axis is parallel to the initial plane of the interface. A reversible chemical reaction occurs between the two fluids leading to the formation of a product (C) of viscosity μ_C:

$$A + B \rightleftharpoons C \tag{1}$$

As time proceeds, the bi-molecular reaction results in the accumulation of more chemical product at the interface between the two reactants. This leads to the coexistence of the three chemical species (A) Fig. 1 shows an idealized distribution of the two reactants (A) and (B) and the product (C), with two fronts. One between the reactant (A) and the product (C); (A–C) while the other is between the reactant (B) and the product (C); (C–B), and they are referred to as the trailing and the leading front, respectively. It should be stressed that this is an idealization of the system and the three chemical species are actually present to a more or less

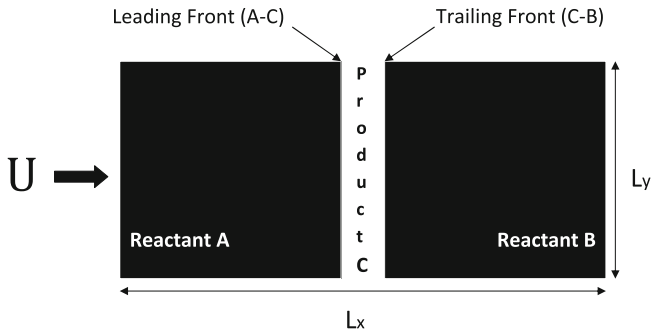

Fig. 1 Schematic of a reactive front displacement process

degree everywhere in the region where the reaction takes place. However, this concept of a leading and trailing front will be helpful in the interpretation and explanation of the results.

2.2 Governing Equations

The flow is governed by the equations for conservation of mass, momentum (Darcy's Equation) and the transport of the three chemical species.

$$\nabla \cdot \mathbf{v} = 0, \tag{2}$$

$$\nabla p = -\frac{\mu}{K}\mathbf{v}, \tag{3}$$

$$\phi\frac{\partial A}{\partial t} + u\frac{\partial A}{x} + v\frac{\partial A}{y} = \phi D_A\left[\frac{\partial^2 A}{\partial x^2} + \frac{\partial^2 A}{\partial y^2}\right] - kAB + k_r C, \tag{4}$$

$$\phi\frac{\partial B}{\partial t} + u\frac{\partial B}{x} + v\frac{\partial B}{y} = \phi D_B\left[\frac{\partial^2 B}{\partial x^2} + \frac{\partial^2 B}{\partial y^2}\right] - kAB + k_r C, \tag{5}$$

$$\phi\frac{\partial C}{\partial t} + u\frac{\partial C}{x} + v\frac{\partial C}{y} = \phi D_C\left[\frac{\partial^2 C}{\partial x^2} + \frac{\partial^2 C}{\partial y^2}\right] + kAB - k_r C. \tag{6}$$

In the above equation, $\mathbf{v} = ui + vj$ is the velocity vector with u and v the $x-$ and $y-$ components respectively, p the pressure, μ the viscosity, K the medium permeability and ϕ its porosity. The concentrations of the two reactants and the product are denoted by A, B and C, respectively while D_A, D_B and D_C are their corresponding diffusion coefficients. Furthermore, k is the reaction constant while k_r represents the reverse reaction constant. For simplicity, it will be assumed that all species have the same diffusion coefficient, i.e. $D_A = D_B = D_C = D$.

Since the characteristic velocity for the fluid flow through the porous medium is U/ϕ, we adopted a Lagrangian reference frame moving at a velocity U/ϕ. Furthermore, diffusive time $D\phi^2/U^2$ and diffusive length $D\phi/U$ are chosen to make the length and time dimensionless. The constant permeability K is incorporated in the expression of the viscosity by treating μ/K as μ, and we shall refer to ratios of μ as either viscosity or mobility ratios. The rest of the scaling is as follows: the velocity is scaled with U/ϕ, the viscosity and pressure with μ_A and $\mu_A D/\phi$, respectively, and the concentration with that of the pure displacing fluid, A_0. The dimensionless equations are:

$$\nabla \cdot \mathbf{v} = 0, \tag{7}$$

$$\nabla p = -\mu(\mathbf{v} + \mathbf{i}), \tag{8}$$

$$\frac{\partial A}{\partial t} + u\frac{\partial A}{x} + v\frac{\partial A}{y} = \left[\frac{\partial^2 A}{\partial x^2} + \frac{\partial^2 A}{\partial y^2}\right] - D_a AB + D_r C, \tag{9}$$

$$\frac{\partial B}{\partial t} + u\frac{\partial B}{x} + v\frac{\partial B}{y} = \left[\frac{\partial^2 B}{\partial x^2} + \frac{\partial^2 B}{\partial y^2}\right] - D_a AB + D_r C, \tag{10}$$

$$\frac{\partial C}{\partial t} + u\frac{\partial C}{x} + v\frac{\partial C}{y} = \left[\frac{\partial^2 C}{\partial x^2} + \frac{\partial^2 C}{\partial y^2}\right] + D_a AB - D_r C. \tag{11}$$

In the above equations, dimensionless variables are represented with asterisk while $D_a = kA_0 D/U^2$ is the Damkohler number representing the ratio of hydrodynamic to chemical characteristic times and $D_r = k_r D/U^2$ represents a reversible Damkohler number. Two additional dimensionless groups are also involved, namely the Péclet number $P_e = UL_x/D$ and the cell aspect ratio $A_r = L_x/L_y$ that appear in the boundary conditions equations.

Following previous studies, an exponential concentration dependent viscosity model is adopted to complete the model [8, 10, 24],

$$\mu = \exp(R_b B + R_c C) \tag{12}$$

where R_b and R_c are the log-mobility ratios between the species as follows:

$$R_b = \ln\left(\frac{\mu_B}{\mu_A}\right) \quad and \quad R_c = \ln\left(\frac{\mu_C}{\mu_A}\right) \tag{13}$$

An associated mobility ratio at the chemical front between the chemical product (C) and the reactant (B), and between the reactant (A) and the product (C) can be also defined as:

$$R_{AC} = \ln\left(\frac{\mu_C}{\mu_A}\right) = \frac{R_c}{2} \quad and \quad R_{CB} = \ln\left(\frac{\mu_B}{\mu_C}\right) = R_b - \frac{R_c}{2} \tag{14}$$

It should be stressed here that the different fronts, whether it is the initial reactive front between (A) and (B) or the idealized leading and trailing ones will

be unstable whenever their mobility ratios are strictly positive, while they will be stable if the mobility ratios are negative or zero. For convenience, in all that follows, the asterisks will be dropped from all dimensionless variables.

2.3 Numerical Techniques

The above problem is formulated using a stream-function vorticity formulation, where the velocity field, the streamfunction ψ and the vorticity ω are related as:

$$u = \frac{\partial \psi}{\partial y}, \quad v = -\frac{\partial \psi}{\partial x}, \quad \nabla^2 \psi = -\omega. \tag{15}$$

where ∇^2 is the Laplacian operator.

The pressure term is eliminated by taking the curl of Eq. (8) resulting in the following relationship between the vorticity and the concentrations of the three chemical species:

$$\omega = R_b \left(\frac{\partial \psi}{\partial x}\frac{\partial B}{\partial x} + \frac{\partial \psi}{\partial y}\frac{\partial B}{\partial y} + \frac{\partial B}{\partial y} \right) + R_c \left(\frac{\partial \psi}{\partial x}\frac{\partial C}{\partial x} + \frac{\partial \psi}{\partial y}\frac{\partial C}{\partial y} + \frac{\partial C}{\partial y} \right) \tag{16}$$

Equations (9)–(11) and (16) form a closed set that can be solved for the concentration and velocity fields. The system of partial differential equation is solved by decomposing the variables as a base-state and a perturbation. The perturbation terms consist of a random noise centered at the initial interface between the reactants A and B, with the magnitude of the noise decaying rapidly away from the interface. The resulting system of three partial differential equations is solved using a highly accurate pseudo-spectral method based on the Hartley transform [4, 10]. This method allows to recast the partial differential equation in time and space into an ordinary differential equation in time. The solution for the time stepping of the reactive-diffusive-convective equations was generated by using a semi-implicit predictor-corrector method along with an operator-splitting algorithm.

3 Result

3.1 Numerical Code Validation

The numerical code has been validated by comparing the time evolution and the related viscous fingers interactions to those presented by Hejazi and Azaiez [10] for the non-reversible case ($\alpha = 0$). It has been noted that the dynamics of fingering were identical when the same parameters were used along with the same spatial resolution and time step size. In addition, the numerical convergence of the

numerical results has also been tested by varying the spatial resolution and the time step. In this study, unless mentioned otherwise, a spatial resolution of 256×256 is used along with a time step dt $= 0.005$.

3.2 Concentration ISO-Surfaces Contours

The dynamics of the flow and the development of the instability are expected to depend on the flow parameters, namely the Péclet number Pe, cell aspect ratio A_r, Damkohler number D_a, reversibility ratio coefficient α as well as the species' mobility ratios; R_b and R_c. Prior to discussing the effects of chemical reversibility, a brief explanation of the effects of chemical reaction on the viscous fingering instability is presented. More details can be found in [10].

3.2.1 Effects of the Chemical Reaction

Figure 2 shows a time sequence of contours of the displacing fluid in the case of non-reactive flow displacement for a mobility ratio of $R_b = 3$. In this case the displaced fluid is more viscous than the displacing one resulting in an unstable front. The finger structures develop and become more complex with time as a result of different mechanisms of interactions that have already been analyzed in the literature.

When chemical reactions take place, the instability is modified and will depend on both mobility ratios R_b and R_c. Figure 3 shows concentration iso-surfaces of the reactant (A) in the case $R_b = 3$, $R_c = 5$, $D_a = 0.5$ and $Pe = 1{,}000$. It is clear that the frontal instability is affected by the reaction resulting in a larger number of fingers that tend to be thinner and to have more complex structures. Figure 4 depicting the corresponding contours for the chemical product (C) shows that the contours of (C) actually allow to illustrate simultaneously the finger structures of the displacing fluid (A) (compare the trailing front in Fig. 4 with those in Fig. 3) and those of the displaced one (B) through the leading front. This indicates that plots of the chemical product contours allow us to show the development of the instability at all fronts, and hence it will be used in all subsequent figures. Note that both the leading and trailing fronts are unstable. Furthermore, as time proceeds and more product is generated, the fingers develop more and extend both upstream and downstream.

In what follows, the effects of chemical reversibility are analyzed. Given the large number of parameters and the fact that the effects of the Péclet number and Damkohler numbers have already been analyzed in the case of irreversible reactions, a number of parameters will be fixed in order to focus the analysis on the role of chemical reversibility. In all that follows, the aspect ratio, Péclet number and Damkohler number are fixed as $A_r = 2$, $P_e = 1{,}000$ and $D_a = 1$. Furthermore, since the dynamics of the flow depend on the mobility ratios, the results will be discussed first for systems that involve an initially stable front between the two

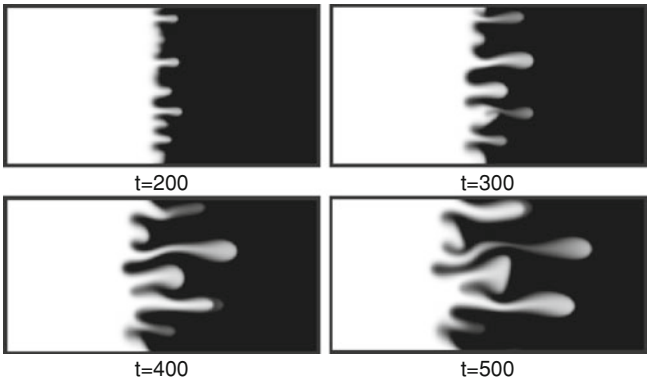

Fig. 2 Contours of (A) for a non-reactive flow: $R_b = 3$

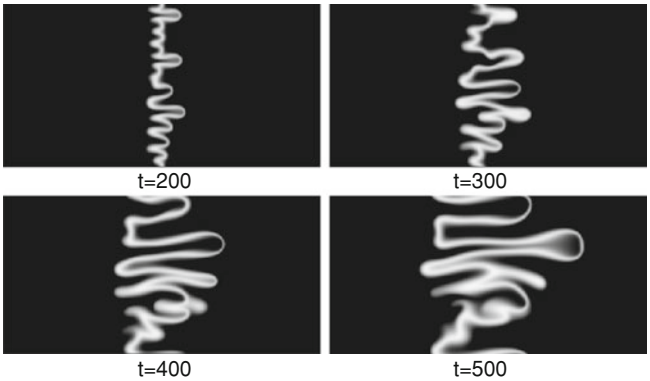

Fig. 3 Contours of (A) for a reactive flow: $R_b = 3$, $R_c = 5$, $D_a = 0.5$

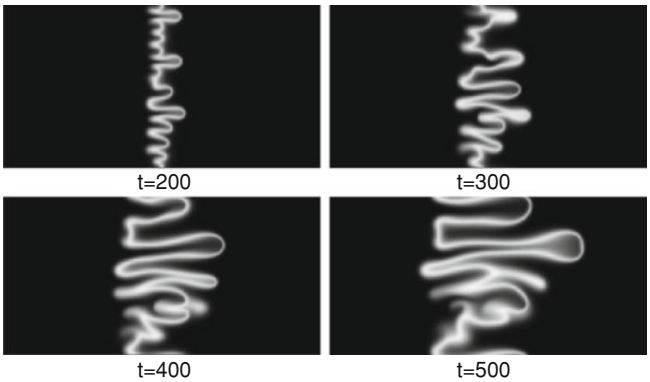

Fig. 4 Contours of the chemical product (C) for a reactive flow: $R_b = 3$, $R_c = 5$, $D_a = 0.5$

reactants ($R_b \leq 0$) followed by that where the initial front is unstable ($R_b > 0$). All qualitative results are presented in the form of concentration iso-surfaces of the chemical product (C).

3.2.2 Stable or Neutrally Stable Initial Interface ($R_b \leq 0$)

The initial interface between the two reactants is stable or neutrally stable if the viscosity of the displacing fluid is larger than or equal to that of the displaced one ($R_b \leq 0$). However, as the reaction takes place and chemical product is generated, instability may develop at either the trailing or the leading front but not at both. The case where the viscosity of (C) lies between those of (B) and (A) or equal to both or any of them ($\mu_A \geq \mu_C \geq \mu_B$) results in a stable displacement process and therefore, will not be discussed. In what follows, the two cases where instability appears at only the trailing or the leading front are examined.

An unstable trailing front and a stable leading front are observed in the case where the viscosity of (C) is grater than that of both reactants. On the other hand, a stable trailing front and an unstable leading will occur when the viscosity of the product (C) is smaller than the viscosities of both reactants. It is worth mentioning that in these cases, the mixing between the two reactants is mainly controlled by diffusion. As a result, the growth of fingers is rather slow compared to cases with unstable initial fronts.

In such cases involving stable initial reactive fronts, reversibility tends to attenuate the instability at the unstable trailing or leading front and may actually result in a completely stable system for a period of time. Figure 5 depicts the case where the instability takes place at the trailing front when the chemical reaction is complete ($\alpha = 0$), while the instability of the system decreases when the reaction reverses ($\alpha \neq 0$). This can be attributed to the fact that in the initial stages of the flow, the mixing of the different species is governed by diffusion and reversibility perpetuates this state by preventing more of the product to accumulate and to trigger instability at the unstable front. However, the amount of chemical product will still keep growing with time, though slowly, and instability will eventually appear at the unstable trailing front at later times (see Fig. 5). The time for the instability to appear depends on the rate of chemical reversibility, with smaller reversibility coefficients leading to an earlier growth of fingers. This time also depends on the mobility ratios of the different chemical species, with distributions that lead to a more unstable trailing front resulting in the instability developing earlier in time. To illustrate this, the results for ($R_b = -1.0$, $R_c = 5$, $R_{AC} = 2.5$) depicted in Fig. 6 show that the instability develops earlier in time in comparison with the case in Fig. 5 where $R_{AC} = 1.5$. Similar conclusions were reached for the case where the instability takes place at the leading front, and for brevity the corresponding contours are not shown.

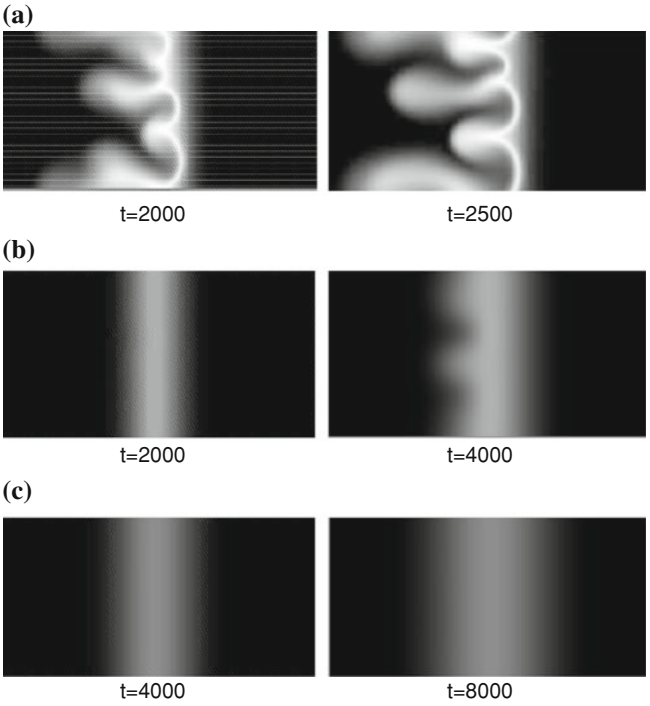

Fig. 5 Concentration iso-surfaces for $R_b = -1$, $R_c = 3$ (unstable trailing front, stable leading front): **a** $\alpha = 0.0$, **b** $\alpha = 0.3$, **c** $\alpha = 0.8$

Fig. 6 Concentration iso-surfaces for $\alpha = 0.3$, $R_b = -1$, $R_c = 5$ (unstable trailing front, stable leading front)

3.2.3 Unstable Initial Interface ($R_b > 0$)

When a less viscous fluid (A) is used to displace another one (B) with a higher viscosity, the initial interface between the two fluids is unstable ($R_b > 0$). The viscosity of the chemical product (C) can be either smaller than, larger than or in between the viscosities of (A) and (B). As a result, regardless of the viscosity of the product (C), instability will take place at least at the trailing or the leading front, if not at both. In what follows, various cases of instability are discussed.

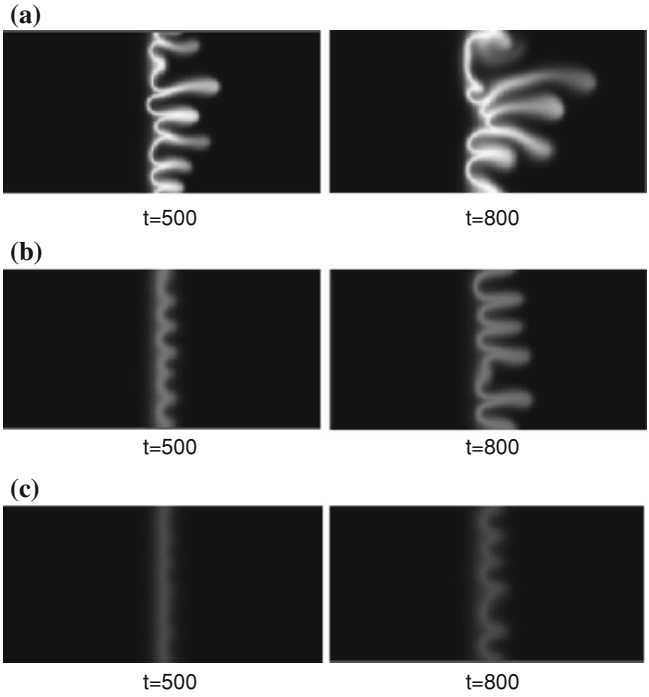

Fig. 7 Concentration iso-surfaces $R_b = 1$, $R_c = -2$ (stable trailing front and unstable leading front): **a** $\alpha = 0.0$, **b** $\alpha = 0.3$, **c** $\alpha = 0.8$

Concentration contours of the chemical product (C) are depicted in Fig. 7 for the case where the product's viscosity is smaller than those of both reactants; i.e. $R_{AC}(=R_c/2) < 0$ and $R_{CB}(=R_b - R_c/2) > 0$. The results are presented for the cases where the chemical reaction is complete ($\alpha = 0$), weakly reversible ($\alpha = 0.3$) and strongly reversible ($\alpha = 0.8$). It is worth noting that in all three cases the instability develops mainly on the leading front and the fingers extend in the downstream direction. Furthermore, it is clear that in this case reversibility tends to attenuate the instability of the flow. In particular, fingers are less developed and more diffuse than in the non-reversible case. However, reversibility also increased the number of developed fingers. Moreover, it should be noted that the distribution of the chemical product is more homogeneous and shows less gradients than in the non-reversible reaction flow. This indicates that in such reversible-reaction flows, the chemical product is more uniformly distributed in the medium. When the viscosity of the product (C) is larger than those of both reactants, the viscosity ratio will be in favour of the growth of instability at the trailing ($R_c > 0$), but not the leading front ($R_b - R_c/2 < 0$). As a result, fingers appear on the trailing front and extend in the opposite direction of the flow, while the leading front is expected to be stable. Figure 8 depicts the case $R_b = 1$ and $R_c = 3$, which corresponds to unstable trailing and stable leading fronts. It is interesting to note that in this case,

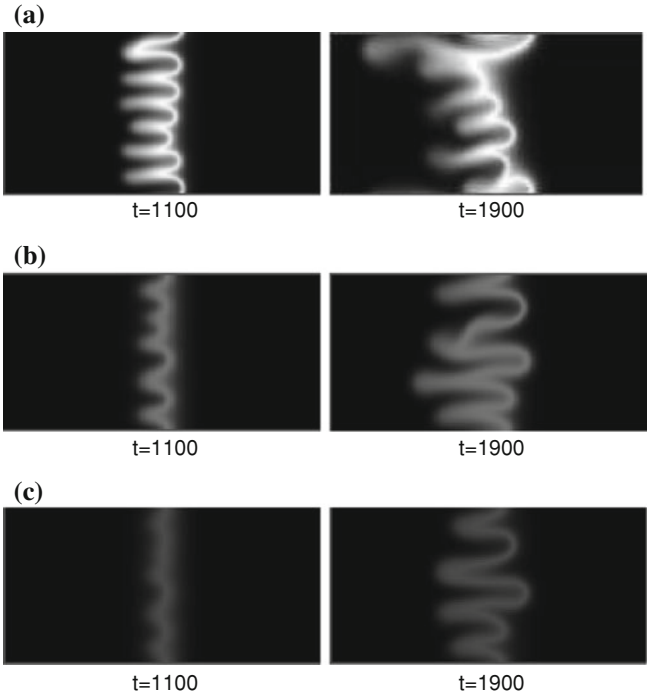

Fig. 8 Concentration iso-surfaces $R_b = 1$, $R_c = 3$ (unstable trailing front and stable leading front): **a** $\alpha = 0.0$, **b** $\alpha = 0.3$, **c** $\alpha = 0.8$

reversibility does actually enhance the instability particularly at the leading front, where the fingers become more developed and narrower with increasing α. Furthermore here too, reversibility leads to a more homogeneous distribution of the chemical product. Figure 9 depict results for reactive flow displacements where the viscosity of (C) lies between those of the two reactants. In this case both the trailing and the leading fronts are unstable ($R_c > 0$, $R_b - R_c/2 > 0$). The non-linear simulations indicate that reversibility does not actually have a major effect on the finger structure, and aside from the fact that the chemical product is more uniformly distributed in the porous medium when the reaction reverses, the number and overall structures of fingers are virtually unchanged. It should be finally noted that in all previous cases where the initial reactive front is unstable, stronger reversibility systematically leads to thinner and less diffuse fingers with a uniform distribution of the chemical product. The previous results can be explained by examining the effects of the chemical reversibility on the distribution of the viscosity on the different fronts. First, it should be noted that in a reactive displacement process, instability will not grow until a certain amount of the product (C) is generated. Furthermore, for the unstable initial reactive front case ($R_b > 0$) when the instability develops at one of the trailing or the leading fronts,

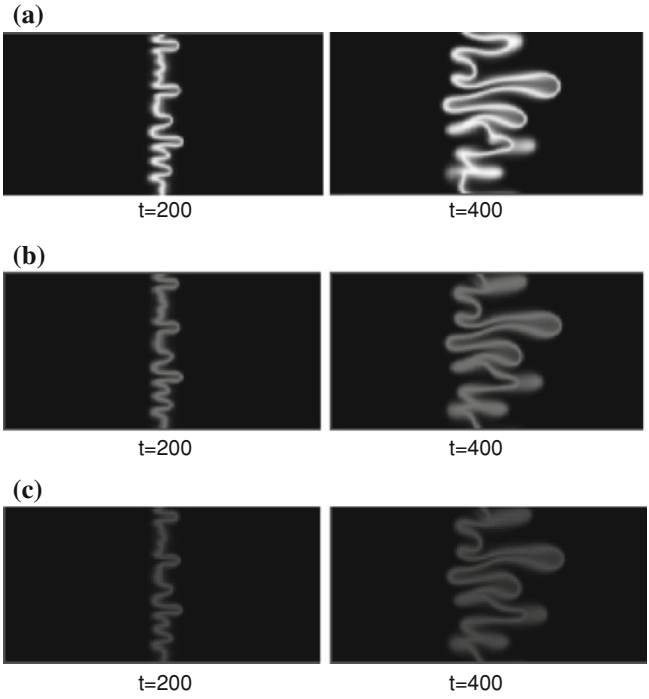

Fig. 9 Concentration iso-surfaces $R_b = 3$, $R_c = 4$ (unstable trailing and leading fronts): **a** $\alpha = 0.0$, **b** $\alpha = 0.3$, **c** $\alpha = 0.8$

the mobility ratio at that unstable front is always larger than that of the initial reactive front. As the reaction reverses and (C) is converted back into (A) and (B), the favourable mobility ratio between the reactants will increase and decrease the mobility ratios at the stable and the unstable front, respectively. Furthermore, it is known that the direction of injection is in favour of the growth of the instability at the leading (C–B), but not the trailing (A–C) front [15]. These two factors explain the influence of reversibility in attenuating or enhancing the instability of the cases where the instability developed at the leading ($R_b = 1, Rc = -2$ and $R_{CB} > R_b$) or the trailing ($R_b = 1$, $R_c = 3$ and $R_{CB} < R_b$) front, respectively.

The less noticeable effects of reversibility in Fig. 9 corresponding to ($R_b = 3$, $R_c = 4$, $R_{AC} = 2$, $R_{CB} = 1$) can be attributed to the fact that in this case the trailing and leading fronts are unstable, resulting in a stronger mixing of the chemical species. Furthermore, the favorable mobility ratio between the reactants (R_b) increases the mobility ratios at both the trailing and the leading fronts as the reaction reverses. This helps the instability to keep growing regardless of how fast the product (C) is converted back to (A) and (B).

4 Conclusion

In this study, the nonlinear development of fingering instabilities that develop in reactive flow displacements in porous media is examined. The study has in particular focused on the effects of chemical reversibility in bi-molecular reactions that affect the viscosity distributions of the three chemical species and in turn the fate of the flow. The study examined the effects of reversibility under the conditions of stable and unstable initial reactive fronts.

Analyses of concentration iso-surfaces of the chemical product revealed that in all flow situations, chemical reversibility tends to lead to a more uniform and homogeneous distribution of the product, when compared with the non-reversible reaction case. Furthermore, foe flows involving an initially stable front between the two chemical reactants, reversibility of the chemical reaction systematically induce an attenuation of the fingering instability. This attenuation was also observed in the case of an initially unstable front between the reactants that result in unstable leading and stable trailing fronts. No noticeable effects were however noted for viscosity distributions that correspond to an unstable initial reactive front with unstable trailing and leading fronts. The only exception where it was found that reversibility can actually enhance the fingering instability is for flows involving an unstable initial front between the two reactants with unstable trailing and stable leading fronts. In this particular case, it was found that the reversibility of the chemical reaction tends actually to enhance the growth of instabilities at the stable leading front. This enhancement can be attributed to the combined effect of the increase of the mobility ratio at the leading front due to the favourable mobility ratio between the initial reactants and the direction of the injection that promotes the growth of the fingers at the leading front.

Acknowledgements H. Alhumade acknowledges financial support from the Ministry of higher education in Saudi Arabia. The authors would like also to acknowledge WestGrid for providing computational resources.

References

1. H. Alhumade, J. Azaiez, In: *Reversible reactive flow displacements in homogeneous porous media*, Lecture Notes in Engineering and Computer Science: Proceedings of The World Congress on Engineering 2013, WCE 2013, 3–5 July, 2013, London, pp. 1681–1686
2. H. Alhumade, J. Azaiez, Stability analysis of reversible reactive flow displacements in porous media. Chem. Eng. Sci. **101**, 46–55 (2013)
3. T. Bansagi, D. Horvath, A. Toth, Nonlinear interactions in the density fingering of an acidity front. J. Chem. Phys. **121**, 11912–11915 (2004)
4. R.N. Bracewell, *The Fourier Transform and its Applications*, 2nd edn. (McGraw Hill, New York, 2000)
5. B. Chopard, M. Droz, T. Karapiperis, Z. Racz, Properties of the reaction front in a reversible reaction-diffusion process. Phys. Rev. E **47**, R40–R43 (1993). Statistical Physics, Plasmas, Fluids, and Related Interdisciplinary Topics

6. A. De Wit, G.M. Homsy, Nonlinear interactions of chemical reactions and viscous fingering in porous media. Phys. Fluids **11**, 949–951 (1999)
7. A. De Wit, G.M. Homsy, Viscous fingering in reaction-diffusion systems. J. Chem. Phys. **110**, 8663–8675 (1999)
8. K. Ghesmat, J. Azaiez, Miscible displacements of reactive and anisotropic dispersive flows in porous media. Tran. Porous Med. **77**, 489–506 (2009)
9. S. Havlin, D. Ben-Avraham, Diffusion in disordered media. Adv. Phys. **51**, 187–292 (2002)
10. S.H. Hejazi, J. Azaiez, Nonlinear interactions of dynamic reactive interfaces in porous media. Chem. Eng. Sci. **65**, 938–949 (2010)
11. G.M. Homsy, Viscous Fingering in Porous Media. Ann. Rev. Fluid Mech. **19**, 271–311 (1987)
12. D. Horvath, T. Bansagi, A. Toth, Orientation-dependent density fingering in an acidity front. J. Chem. Phys. **117**, 4399–4402 (2002)
13. M.N. Islam, J. Azaiez, Fully implicit finite difference pseudo-spectral method for simulating high mobility-ratio miscible displacements. Int. J. Num. Meth. Fluids **47**, 161–183 (2005)
14. K.V. McCloud, J.V. Maher, Experimental perturbations to Saffman–Taylor flow. Phys. Rep. **260**, 139–185 (1995)
15. M. Mishra, M. Martin, A. de Wit, Miscible viscous fingering with linear adsorption on the porous matrix. Phys. Fluids **19**, 1–9 (2007)
16. Y. Nagatsu, T. Ueda, Effects of reactant concentrations on reactive miscible viscous fingering. Fluid. Mech. Trans. Phen. **47**, 1711–1720 (2001)
17. Y. Nagatsu, T. Ueda, Effects of finger-growth velocity on reactive miscible viscous fingering. AIChE J. **49**, 789–792 (2003)
18. Y. Nagatsu, S. Bae, Y. Kato, Y. Tada, Miscible viscous fingering with a chemical reaction involving precipitation. Phys. Rev. E: Stat., Nonlin., Soft Matter Phys. **77**, 1–4 (2008)
19. H. Nasr-El-Din, K. Khulbe, V. Hornof, G. Neale, Effects of interfacial reaction on the radial displacement of oil by alkaline solutions. Revue—Institut Francais du Petrole **45**, 231–244 (1990)
20. T. Rica, D. Horvath, A. Toth, Density fingering in acidity fronts: Effect of viscosity. Chem. Phys. Lett. **408**, 422–425 (2005)
21. P. Saffman, G. Taylor, The penetration of a fluid into a porous medium or hele-shaw cell containing a more viscous liquid. Proc. R. Soc. Lond. A **245**, 312–329 (1958)
22. M. Sinder, V. Sokolovsky, J. Pelleg, Reversible reaction diffusion process with initially mixed reactants: Boundary layer function approach. Phys. B: Condens. Matter **406**, 3042–3049 (2011)
23. M. Sinder, H. Taitelbaum, J. Pelleg, Reversible and irreversible reaction fronts in two competing reactions system. Nucl. Instrum. Methods Phys. Res. Sect. B **186**, 161–165 (2002)
24. C. Tan, G. Homsy, Simulation of nonlinear viscous fingering in miscible displacement. Phys. Fluids **31**, 1330–1338 (1998)
25. A. Zadrazil, I. Kiss, J. D'Hernoncourt, H. Sevcikova, J. Merkin, A. De Wit, Effects of constant electric fields on the buoyant stability of reaction fronts. Phys. Rev. E **71**, 1–11 (2005)
26. W. Zhang, Nanoscale iron particles for environmental remediation: An overview. J. Nanopart. Res. **5**, 323–332 (2003)

Prediction of Thermal Deformation for a Ball Screw System Under Composite Operating Conditions

A. S. Yang, S. Z. Chai, H. H. Hsu, T. C. Kuo, W. T. Wu, W. H. Hsieh and Y. C. Hwang

Abstract The position error of a feed drive system is mostly caused by thermal deformation of a ball screw shaft. A high-speed ball screw system can generate massive heat with greater thermal expansion produced, and consequently have a negative effect on the positioning accuracy. In this study, we applied the computational approach using the finite element method (FEM) to simulate the thermal expansion process for estimating the deformation of the ball screw system. In the numerical analysis, the deformation of the ball screw shaft and nut was modeled via a linear elasticity approach along with the assumption that the material was elastic, homogeneous, and isotropic. To emulate the reciprocating movements of the nut at the speeds of 20, 40 and 60 m/min corresponding to the screw shaft, we also employed a three-dimensional unsteady heat conduction equation with the heat generation from the main sources including the ball screw shaft, nut and bearings as the heat transfer model to solve the temperature distributions for determining the temperature rises and axial thermal deformations in a ball screw

A. S. Yang · S. Z. Chai · H. H. Hsu
Department of Energy and Refrigerating Air-Conditioning Engineering, National Taipei University of Technology, Taipei 106, Taiwan
e-mail: asyang@ntut.edu.tw

T. C. Kuo · W. H. Hsieh (✉)
Department of Mechanical Engineering, and Advanced Institute of Manufacturing with High-tech Innovations, National Chung-Cheng University, Chiayi 621, Taiwan
e-mail: imewhh@ccu.edu.tw

W. T. Wu
Department of Biomechatronics Engineering Nation Pingtung University of Science and Technology, Pingtung 912, Taiwan
e-mail: azbennywu@gmail.com

Y. C. Hwang
HIWIN Technologies Corp, Taichung 408, Taiwan
e-mail: lawrence@mail.hiwin.com.tw

G.-C. Yang et al. (eds.), *Transactions on Engineering Technologies*,
DOI: 10.1007/978-94-017-8832-8_2,

shaft under composite operating conditions. The simulated results demonstrated that the countermeasures must be taken to thermally compensate great deterioration of the positioning accuracy due to vast heat production at high rotating speeds of shaft for a ball screw system.

Keywords Ball screws · FEM · Heat transfer model · Machine tool · Positioning accuracy · Thermal deformation

1 Introduction

The performance of a ball screw feed drive system in terms of speed, positioning accuracy and machine efficiency plays a very important role in product quality and yield in manufacturing industries primarily including machine tools, semi-conductors, optoelectronics, and so on. Considering a high-speed precision ball screw system, the occurrence of contact surfaces (such as the interfaces between the ball and nut grooves, the ball and screw grooves, and the bearing and shaft) produces contact friction at these junctions. The friction of the nut and ball bearings entails a sudden and violent heating of balls, and in turn results in the temperature rises of the ball screw, leading to mechanical micro- deformations and an overheating of the coolant. Such a temperature heating of ball screw could also cause significant thermal deformations deteriorating the ball screw system accuracy in mechatronics tools or instruments [1].

The development of fabrication technology for a variety of applications necessitates high-precision apparatuses for achieving remarkably delicate goods with high output [2]. As indicated by Bryan [3], the thermal induced error in precision parts has still been the key setback in the industry. Substantial efforts were done on the machine tools, thermal behavior and thermal error compensation on the spindles, bearings and ball screws, respectively. Ramesh et al. [4] and Chen [5] carried out the air-cutting experiments to reproduce the loads under actual-cutting situations. To adjust the thermal conditions of the machine tool, Li et al. [6] conducted the tests of varying spindle speed for controlling the loads. The performance of a twin-spindle rotary center was experimentally evaluated by Lo et al. [7] for particular operating settings. Afterward, Xu et al. [8] incorporated the contact resistance effect into a thermal model for simulation of machine tool bearings. Koda et al. [9] produced an automatic ball screw thermal error compensation system for enhancement of position accuracy.

The frictional process from a high-speed ball screw system essentially released tremendous amounts of heat and results in the continuing temperature increase and thermal expansion, leading to deterioration of the positioning accuracy. In this investigation, we considered the heat generation from two bearings and the nut as the thermal loads with the prescribed heat flux values imposed on the inner surfaces of grooves between the bearings and nut of the ball screw system.

The convection boundary conditions were also treated for solid surfaces exposed to the ambient air. A FEM-based thermal model was developed to resolve the temperature rise distribution and in turn to predict the thermal deformation of the ball screw. In addition, simulations were conducted to appraise the influence of composite operating conditions in terms of different speeds (1,000, 2,000 and 3,000 rpm) as well as moving spans (500 and 900 mm) of the nut on the temperature increases and thermal deformations of a ball screw shaft.

2 Description of Ball Screw System

Figure 1 presents a schematic diagram of a ball screw feed drive system, encompassing a ball screw and driving unit. A continuous advance and return movement of the ball screw takes place in the range of 900 mm. It has 20-mm lead, 41.4-mm ball center diameter (BCD) and 1,715-mm total length. The outer and inner diameters of the screw shaft are 40 and 12.7 mm, respectively. Table 1 presents the parameters of main components for the ball screw drive system, which really contains the ball screw shaft, ball screw nut and bearings.

Figure 2 illustrates the moving velocity of the screw nut. This investigation considers the reciprocating movements of the nut at a maximum speed of 40 m/min pertaining to the screw shaft with a time period of 3.43 s and acceleration/deceleration of ± 2.1 m/s^2 as the baseline study case.

3 Computational Analysis

The physical model in this study investigates the thermal expansion process in a ball screw system. Essentially, heat is generated mainly from the friction between the ball and nut grooves as well as the ball and screw grooves. In view of the fact that a string of balls filled the grooves between the screw and nut are rotating very fast, the heat has been distributed evenly over the inner surface of raceways. The nut and two bearings are modeled as the fixed thermal loads imposed on the ball screw shaft. The thermal resistance resulting from the lubrication oil film between the balls and raceways is assumed to be ignored here attributable to a very thin layer of oil film, and the effect of heat conduction by means of the lubricant and thermal deterioration is negligible. Numerical calculations were performed by the FEM software ANSYS® to investigate the thermal behavior of a ball screw [10]. The theoretical formulation was based upon the time-dependent three-dimensional heat conduction equation for a ball screw system. The governing equations are stated as follows:

$$k\left(\frac{\partial^2 T}{\partial x^2}+\frac{\partial^2 T}{\partial y^2}+\frac{\partial^2 T}{\partial z^2}\right)=\rho c\frac{\partial T}{\partial t}. \tag{1}$$

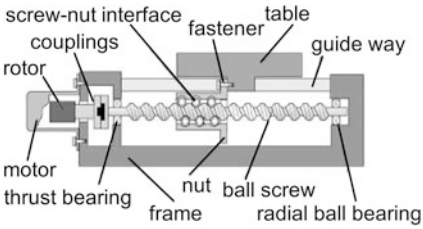

Fig. 1 Schematic of a ball screw feed drive system

Table 1 Main component parameters of the ball screw feed drive system

Ball screw shaft		Ball screw nut	
Total Length (mm)	1,715	Type	FDC
Thread Length (mm)	1,295	Length (mm)	143.4
LEAD (mm)	20	Diameter (mm)	70
BCD (mm)	41.4		
Outer diameter(mm)	40		
Inner diameter (mm)	12.7	*Bearing*	
Line number	2	Type	TAC
Contact type	4 points	OD (mm)	30
Ball diameter (mm)	6.35	ID (mm)	12.7

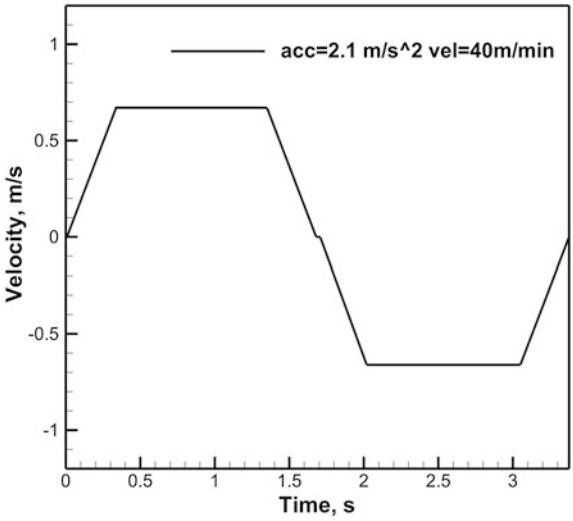

Fig. 2 Moving velocity of the screw nut with respect to the screw shaft

The symbols ρ, c, k and T mean the density, specific heat, thermal conductivity, and temperature of the ball screw shaft and nut, respectively. Here the temperature T is a function of the spatial coordinates (x, y, z) and time. The ρ, c, k values for computations are 7,750 kg/m^3, 480 J/kg-^{o}C and 15.1 W/m-^{o}C. Figure 3 exhibits the heat generation by the nut and bearing for a period of 3.43 s. The friction effect

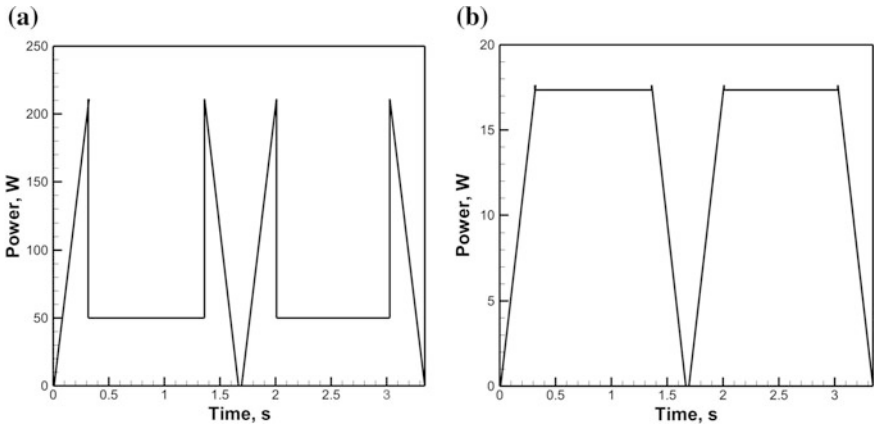

Fig. 3 Heat generation by **a** nut and **b** bearing for a period of 3.43 s

between the balls and raceways of the nut and bearings is the most important cause for temperature increase.

Given that the load of the nut contains two parts: the preload and dynamic load, $\dot{G}_{nut}$, the heat generation by the nut (in W), can be described as [11, 12]:

$$\dot{G}_{nut} = 0.12\pi f_0 v_0 nM. \tag{2}$$

Here f_0 is a factor determined by the nut type and lubrication method; v_0 is the kinematic viscosity of the lubricant (in m^2/s); n is the screw rotating speed (in rpm); M is the total frictional torque of the nut (in N-mm). In this research, $\dot{G}_{bearing}$ is the heat generated by a bearing (in W), defined as below [13].

$$\dot{G}_{bearing} = 1.047 \times 10^{-4} nM. \tag{3}$$

The variables n is the rotating speed of a bearing and M is the total frictional torque of bearings, including the frictional torque due to the applied load and the frictional torque due to lubricant viscosity.

The convective heat transfer coefficient h (in $W/m^2\text{-}^oC$) is computed [14] by

$$h = Nuk_{fluid}/d. \tag{4}$$

Here Nusselt number $Nu = 0.133Re^{2/3}Pr^{1/3}$, while the variables Re and Pr represent Reynolds number and the Prandtl number. The sign k_{fluid} is the thermal conductivity of the surrounding air and d is the outer or inner diameter of the screw shaft (mm). More detailed information can be found in Ref. [15].